LAWRENCE
LIVERMORE
NATIONAL
LABORATORY

LLNL-JRNL-579437

Developing an Approach for First-principles Catalyst Design: Application to Carbon Capture Catalysis

H. J. Kulik, S. E. Wong, S. E. Baker, C. A. Valdez, J. H. Satcher, R. D. Aines, F. C. Lightstone, J. H. Satcher, R. D. Aines, F. C. Lightstone

September 6, 2012

Acta Crystallographica Section C

Disclaimer

Developing an approach for first-principles catalyst design: application to carbon capture catalysis

Heather J. Kulik[a,1], *Sergio E. Wong*[a], *Sarah E. Baker*[a], *Carlos A. Valdez*[a], *Joe H. Satcher, Jr.*[a], *Roger D. Aines*[a] *and Felice C. Lightstone*[a,b]

[a]Bioscience and Biotechnology Division, Lawrence Livermore National Laboratory, 7000 East Ave, Livermore, CA 94550, USA

[b] Corresponding author: Address: 7000 East Ave, Livermore, CA 94550, USA, Email: lightstone1@llnl.gov. Phone: 925-423-8657. Fax: 925-424-5513.

Abstract: An approach to catalyst design is presented in which we first build local potential energy surface models to elucidate design principles and then use these models to identify larger scaffold motifs that match the target geometries. Carbon sequestration via hydration is used as the model reaction, and three- and four- coordinate sp^2 or sp^3 nitrogen ligand motifs are considered for Zn(II) and Co(II) metals. The comparison of binding, activation, and product release over a large range of interaction distances and angles

---

[1] Present address: Department of Chemistry, Stanford University, 333 Campus Drive, Stanford, CA 94305, email: hkulik@stanford.edu

suggests that four-coordinate, short Zn(II)-nitrogen(sp^3) bond distances favor rapid turnover for CO_2 hydration. This design strategy is confirmed first by computationally characterizing [2]the reactivity of a known mimic over a range of metal-nitrogen bond lengths. A search of existing catalysts in a chemical database reveals structures that match the target geometry from model calculations, and subsequent calculations have identified these structures as potentially effective for CO_2 hydration and sequestration.

Keywords: Catalyst design, CO_2 capture, carbonic anhydrase mimics, density functional theory, potential energy surfaces, reaction coordinates, zinc.

1. Introduction

The rational design of small-molecule, transition-metal catalysts has an impact in fields ranging from energy science[1, 2] to pharmaceuticals[3]. The sequestration of carbon dioxide (CO_2) in industrial processes to reduce emission of greenhouse gases[4] is one example of a key challenge that can be addressed through the design of new catalysts. Industrial separations of CO_2 typically rely on converting CO_2 gas to carbonic acid in a liquid phase[5] and then subsequent removal of the liquid fraction, where the formation of carbonic acid is rate limiting[5]. Acceleration of carbonic acid formation through the use of catalysts would improve the effectiveness of these industrial separation processes[6].

---

[2] Abbreviations: CAII – Human carbonic anhydrase, PES – potential energy surface, PBE – Perdew-Burke-Ernzerhof exchange correlation functional, CSD – Cambridge Structural Database.

The enzyme human carbonic anhydrase (CAII) rapidly converts CO_2 to bicarbonate at a zinc metal center (turnover is ~10^6 sec^{-1} at pH 9 and 25° C)[6, 7]. The environment around the Zn center is tetrahedral with three chelating His residues and the fourth site is occupied by a catalytically relevant hydroxide[8-11]. Additional features of the enzyme include a hydrophobic portion responsible for CO_2 binding and a hydrophilic side that facilitates the binding and deprotonating of water. Several small molecule CAII mimetics exist[12], which primarily aim to replicate the Zn center and His ligands of the enzyme active site with a Zn metal ligated by comparable nitrogen electron donors, such as imidazoles[13] and secondary amines[14, 15]. Both carbonic anhydrase and its mimics are believed to form bicarbonate via oxidative attack of CO_2 by the Zn-OH moiety. The newly formed bicarbonate is then displaced by a water molecule, which is deprotonated to regenerate the active hydroxide intermediate[16].

Existing CAII mimics catalyze CO_2 hydration at rates much slower than the native enzyme, and, in this work, we focus on developing a new strategy for identifying CAII mimics that have the potential to exceed turnover rates of those mimics already reported in the carbon capture literature. A number of other metals can bind to carbonic anhydrase[17], and replacing Zn with Co maintains near-wildtype activity in the enzyme[18]. These activity results suggest the exploration of alternative transition metals as an avenue to modulating carbonic anhydrase mimic behavior, but the clear advantage of Zn in particular, both natively and in mimics, is its relative inertness against oxidative stress[19].

Computational design of catalysts can augment experimental efforts to screen and design new catalyst mimics[20]. While computational approaches are much cheaper than

comparable experimental screens[21], the accuracy of the electronic structure methods that can be applied to studying the system sizes typical for molecular catalysts has limited the application of computational approaches. Nevertheless, locality in transition-metal chemistry (the strong dependence of a transition metal center's electronic structure on the character of directly bonded atoms) has long been exploited[22] to study smaller model catalysts than are typically used in industrial settings. Shortcomings in the accuracy of the chosen electronic structure method may be ameliorated somewhat by focusing on relative trends, which are more robust from error cancellation, rather than absolute values.

We believe that methods which examine relative trends in small model systems with minimal ligands, once verified against larger realistic catalysts, should provide a wealth of information. This information may then be used for searches of existing catalysts in structural databases or for the creation of never-before studied catalysts that have desirable characteristics. Carbon capture provides an excellent test case for such alternative computational design methods for two principle reasons: 1) there is a significant difference in the activity of previously characterized model catalysts and native enzymes and 2) there are relatively few apparent reaction steps that will need to be studied and optimized. If optimization strategies for catalysis can be obtained from the computed electronic structure trends on small models, then computation will be better able to serve to guide catalyst selection for experimental study in a variety of relevant chemical reactions.

Here, we present an alternative computational approach to designing catalysts for carbon capture. We have developed extensive potential energy-based reactivity maps for key components of the CO_2 hydration reaction using both three- and four-fold coordinated

metal-nitrogen complexes (sp^2 or sp^3 nitrogen) with both Zn(II) and Co(II) metals. We present results on optimization strategies for the primary aspects of the CO_2 hydration reaction: hydroxyl intermediate formation, CO_2 activation and conversion, and product release. We identify the metal-ligand sets that provide the best activity at equilibrium geometries as well as the sets that are most easily optimized, as determined by characteristics all improving along the same vector of geometric change. We verify the validity of our minimal model by constraining an experimentally-characterized carbonic anhydrase mimic and studying changes in its electronic structure under the constraint to check for correlation against the minimal model potential energy surface (PES) maps. Finally, we characterize catalysts from the literature that both meet and fail to meet the geometric targets obtained from our PES and compare the resulting catalytic properties against a previously characterized carbonic anhydrase mimic.

2. Computational Methods

Density functional theory calculations were carried out using the QUANTUM-ESPRESSO package[23]. An ultrasoft plane-wave pseudopotential approach was used with a cutoff of 30 Ry for the wavefunction and 300 Ry for the density. The pseudopotential for Zn included both semi-core 3*d* and valence 4*s* in the valence. The Perdew-Burke-Ernzerhof (PBE) exchange-correlation functional[24] was used for all calculations since previous work[25] showed that augmenting functionals with a Hubbard U term has little effect on Zn. For Co, an average U of 3.0 eV obtained from linear response across all intermediates was applied. Potential energy surfaces were calculated via constrained relaxations in which the metal-nitrogen distance and the distance of the metal

from the plane of nitrogen atoms was fixed at different values while all other variables were permitted to relax. In each case, stable intermediates were energy minimized under constraint of both bond distance (M-L) and the dihedral formed by the metal with three of its ligands, while all other degrees of freedom were relaxed. The M=Co,Zn and L=NH_3 PES calculations were carried out over a very wide range of M-L distances (1.75-2.55 Å, in 0.05 Å increments) and M-3L dihedrals (0-55°, in 5° increments). Select additional calculations for M=Zn and L=NH_2 were carried out over shorter M-L distance ranges (1.85-2.35 Å, in 0.05 Å increments) and M-4L dihedral ranges (0-40°, in 5° increments). For reference, the lowest energy or equilibrium point of most intermediates on these PESs reside around 2.1 Å and 10° for the dihedral. The energetics of the squeezed catalyst were determined by fixing only the metal-nitrogen distance and allowing everything else to relax. Makov-Payne corrections[26] to the total energy were used when comparing systems of different charge (+1 overall for most reactants and intermediates, +2 for intermediates with axial water and carbonic acid or with no axial ligand, and charges are shifted net negative by one to allow for singlet spin in the case of Zn(II)-3(NH_2)); if the charge remained the same, the systems were treated without the Makov-Payne correction. The candidate structures of putative carbonic anhydrase mimics were obtained by searching data available in the Cambridge Structural Database (CSD)[27] using the Conquest program[28] using constraints on the number and character of ligands coordinating the metal center as well as the metal identity.

3. Results and Discussion

We have characterized a model reaction coordinate for carbon capture via CO_2 hydration in order to identify how to optimize catalysts towards facilitating this reaction. The characteristics of the reaction coordinate (see Fig. 1) were identified as:

1) stability of hydroxyl formation and binding:

$\Delta E_{M-OH} \approx \left[E_{M-OH} + E_{H_3O^+}\right] - \left[E_{M-H_2O} + E_{H_2O}\right]$;

2) activation energy for M-OH attack on CO_2:

$E_a \approx \left[E_{TS(M-HCO_3)}\right] - \left[E_{M-OH} + E_{CO_2}\right]$;

3) reaction energetics for M-OH attack on CO_2:

$\Delta E_{rxn} \approx E_{M-HCO_3} - \left[E_{M-OH} + E_{CO_2}\right]$;

4) product release:

$D_e(P) \approx \left[E_{M-H_2O} + E_{H_2CO_3}\right] - \left[E_{M-H_2CO_3} + E_{H_2O}\right]$.

There are a few assumptions made in our definition of reaction characteristics. In step one, we assume that the axial water ligand is deprotonated to form a hydroxyl via another water molecule. This approximation is justified because trends in hydroxyl formation across geometries are not particularly sensitive to the role and identity of the species that deprotonates. In step four, we assume that a neutral carbonic acid molecule is formed in order to aid its release from the catalyst and that a free water molecule is present and may displace a neutral carbonic acid molecule.[3]

---

[3] In the limit of low pH, carbonic acid is stable and this assumption likely mimics the actual mechanism for product release[29]. For neutral to high pH, carbonic acid species are not in high concentration at equilibrium; nevertheless, short-lived carbonic acid species that dissociate at lower energetic cost are known to form transiently, regardless of the predominance of carbonate or dissolved CO_2 at equilibrium[30]. Additionally, carbonate

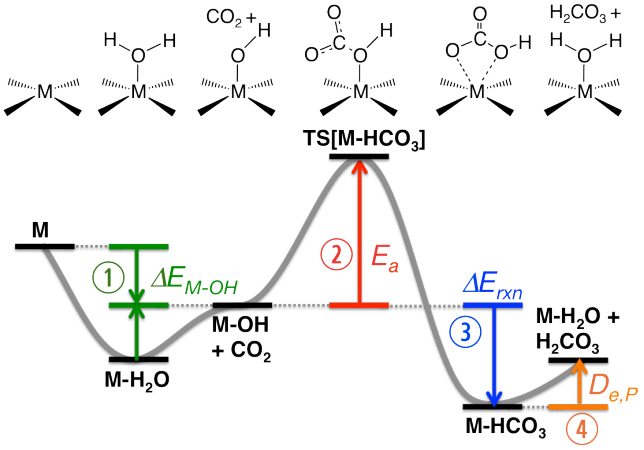

Figure 1. Schematic of reaction characteristics labeled as follows: 1) $\Delta E_{M\text{-}OH}$: hydroxyl stability (green), 2) E_a: activation energy (red), 3) ΔE_{rxn}: reaction energetics (blue), and 4) $D_{e,P}$: product release (orange). Approximate structures are provided above each intermediate.

In order to identify the best strategy for optimizing catalysts for CO_2 hydration, we considered both varying metal and ligand identity and coordination number as well as the geometry of those metals and ligands. Namely, we consider both Co(II) and Zn(II) metals

---

salts[29] may be more common at high pH as well and the assumptions we make about the mechanism of release via exchange of neutral carbonic acid and water hold for the exchange of carbonate salts and water as well. The motivation for studying neutral carbonic acid is due to the well-known poor accuracy in electronic structure methods in describing the dissociation of charged species (bicarbonate is negatively charged and the catalyst is positively charged)[31-40], despite the fact that carbonic acid is in low concentrations in aqueous solutions. Because the focus is on trends, the ease with which a water molecule may displace a carbonic acid molecule provides a sufficient relative metric of product release. We also note that some of the challenges for density functional theory in correctly describing charge transfer may be alleviated when explicit or implicit solvent is incorporated into simulations[41], but that alternative approach is outside the scope of this work.

either four- or three-fold coordinated with ligands (L=NH_3,NH_2 for Zn, L=NH_3 for Co). The ligands were chosen to represent sp^2 (L=NH_2) and sp^3 (L=NH_3) nitrogen atoms, and they coordinated the metal in either a three-fold, trigonal planar to tetrahedral-like geometry or a four-fold, square-planar geometry. The tetra-aza scaffold we later discuss in detail is an example of a scaffold that chelates metals with an sp^3 nitrogen ligand set. The sp^2 nitrogen ligands approximately model ligand sets including imidazole rings or porphines, but we note that it is possible that some features of sp^2 nitrogen atoms in aromatic rings that might be missed by our minimal model[42]. The metals were chosen on the basis of the metal bound in wild type carbonic anhydrase as well as the activity of alternative metals when bound to carbonic anhydrase[43-46]. For each metal and ligand set, full potential energy surfaces were obtained for all the intermediates and transition states that make up the reaction coordinate in Fig. 1 by varying both M-L distance ($D_{M\text{-}L}$) and M-3L dihedral ($\theta_{M\text{-}3L}$).[4] Once these PESs are analyzed for geometric properties that optimize the reaction coordinate, structures that fit these characteristics from the literature will be fully characterized (Fig. 2). The benefits of carrying out a literature search are two-fold: 1) if we confine ourselves initially to previously characterized structures, then the potential catalysts may straightforwardly be synthesized and tested and 2) without restricting ourselves to carbon capture catalysts, we may identify structures relevant to other reactions that may be repurposed for CO_2 hydration.

---

[4] Breaking symmetry via alternating short and long bonds was pursued in a preliminary fashion and not observed to significantly alter broad trends, but further examination may be of interest in future work.

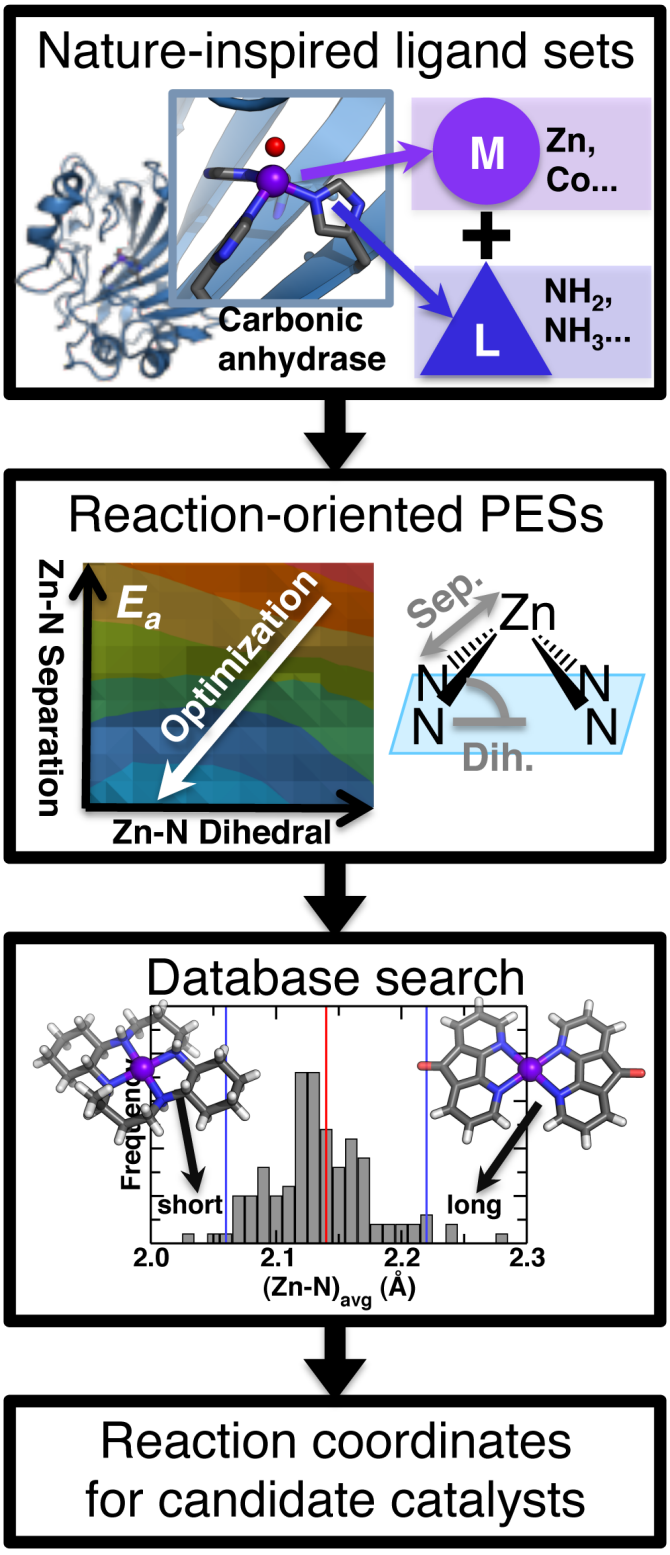
Nature-inspired ligand sets
M
Zn,
Co...
+
L
NH2,
NH3...
Carbonic
anhydrase
Reaction-oriented PESs
Zn-N Separation
Ea
Optimization
Zn-N Dihedral
Sep.
Zn
N
N
N
N
Dih.
Database search
Frequency
short
long
2.0
2.1
2.2
2.3
(Zn-N)avg (Å)
Reaction coordinates
for candidate catalysts

Figure 2. Flow chart indicating strategy for carbon capture catalyst design. Starting from top, 1) metals and ligands are chosen based on enzyme, 2) the dependence of reaction parameters on metal-ligand interaction geometry is explored, 3) reaction-oriented PESs are used as input for a database search, and 4) the reaction coordinate of candidates from the search is obtained.

Using the results of the four properties outlined previously at different fixed distances and dihedrals, we obtained the direction along which the property is optimized when moving from equilibrium (i.e. either shortening or lengthening bonds or flattening or enhancing the dihedral). The results of these optimization directions for all four reaction coordinate characteristics is reported in Table 1 for Zn(II)-ligand sets and Table 2 for Co(II)-ligand sets. For each of the six reaction-oriented PESs we calculated, we obtained equilibrium values of the four reaction characteristics. Using equilibrium data, we observed that hydroxyl formation (point 1) is always favorable, and CO_2 hydration (point 3) is always exothermic (see supporting information). The other two points of consideration, CO_2 hydration barrier height (point 2) and product release (point 4) were instead observed to be energetically costly for all equilibrium points (see supporting information). The absolute values of each point on the intermediate PESs as well as the reaction characteristic PESs are reported in the supporting information for each metal and ligand set.

Table 1. Optimizing structural trends for $D_{M\text{-}L}$ and $\theta_{M\text{-}3L}$ compared over four key reaction characteristics for Zn(II)-4(NH_3), Zn(II)-4(NH_2), Zn(II)-3(NH_2), Zn(II)-3(NH_3). Bond

length ($D_{M\text{-}L}$) optimizing trends are either for short or long bonds. For angles ($\theta_{M\text{-}3L}$) optimizing trends for dihedrals pushing the metal out of the plane of the ligands are indicated as domed, while a preference for an in-plane metal is indicated as flat. In both bond and angle cases, a dash indicates weak or non-monotonic dependence on a given variable.

	Zn(II)-4(NH_3)		Zn(II)-4(NH_2)		Zn(II)-3(NH_3)		Zn(II)-3(NH_2)	
	$D_{M\text{-}L}$	$\theta_{M\text{-}3L}$	$D_{M\text{-}L}$	$\theta_{M\text{-}3L}$	$D_{M\text{-}L}$	$\theta_{M\text{-}3L}$	$D_{M\text{-}L}$	$\theta_{M\text{-}3L}$
$\Delta E_{M\text{-}OH}$	short	flat	short	flat	long	domed	long	domed
E_a	short	flat	long	domed	-	-	-	flat
ΔE_{rxn}	short	flat	-	domed	short	flat	short	domed
$D_{e,P}$	short	flat	short	flat	short	flat	long	domed

Table 2. Reaction property optimizing structural trends for $D_{M\text{-}L}$ and $\theta_{M\text{-}3L}$ compared over four key reaction characteristics for Co(II)-4(NH_3) and Co(II)-3(NH_3). Bond length ($D_{M\text{-}L}$) optimizing trends are either for short or long bonds. For angles ($\theta_{M\text{-}3L}$) optimizing trends for dihedrals pushing the metal out of the plane of the ligands are indicated as domed, while a preference for an in-plane metal is indicated as flat. In both bond and angle cases, a dash indicates weak or non-monotonic dependence on a given variable.

	Co(II)-4(NH_3)		Co(II)-3(NH_3)	
	$D_{M\text{-}L}$	$\theta_{M\text{-}3L}$	$D_{M\text{-}L}$	$\theta_{M\text{-}3L}$
$\Delta E_{M\text{-}OH}$	long	domed	long	domed
E_a	short	-	long	domed
ΔE_{rxn}	long	flat	short	flat
$D_{e,P}$	short	flat	short	flat

We have collected geometric trends for reactivity optimization for each reaction step with a variety of metal-ligand sets (Tables 1 and 2). Steps that are not rate-limiting (e.g. steps 1 and 3 here) should be weighted less in systems where optimization directions differ between different characteristics. Additionally, when comparing multiple metal/ligand sets, even if one set appears to be more easily optimized, the favorability of the reaction coordinates at the metal/ligand sets' respective geometric equilibria should also be compared. Using the two key reaction characteristics, we ranked each metal-ligand set and observed that four-coordinate Zn(II) with L=NH_3 or NH_2 started from the best equilibrium characteristics. For this reason and because Co(II) may be rapidly oxidized to Co(III) under experimental conditions[47], we do not pursue further optimization of cobalt carbon capture catalysts in this work. Instead, we focus on zinc(II)-nitrogen compounds, which are very robust against oxidation[48].

While Zn(II)-$(NH_2)_4$ compounds have more favorable reactivity characteristics at the equilibrium geometry (see supporting information), reaction characteristics are not consistently optimized; hydroxyl binding and product release are optimized by short bonds and flat angles, while the activation energy and reaction energy are optimized by longer bonds and domed angles. Instead, Zn(II)-$(NH_3)_4$ compounds are preferred, because shortened $D_{M\text{-}L}$ and shallower $\Theta_{M\text{-}3L}$ values optimize all reaction properties for this metal-ligand set. We now focus here on using the PES and reaction coordinate optimization data obtained for Zn(II)-$(NH_3)_4$ to both better understand the underlying electronic structure that gives rise to these optimization trends and to validate and verify our approach.

Comparing the results of the Zn-$(NH_3)_4$ PES optimization against a previously computationally-characterized catalyst mimic[49], 1,4,7,10-tetraazacyclododecane (tetra-aza) enables verification of our minimal ligand approach. Using the tetra-aza scaffold with Zn(II) metal center, we carried out structural relaxations for the larger scaffold structures under constrained Zn-N bond distances and examined how the two principal reaction characteristics, activation energy and product release, change with varying Zn-N bond distance[5]. Without constraints, the energy minimized tetra-aza structure has an equilibrium Zn-N bond distance of 2.22 Å. We find that compressing the Zn-N bond in the scaffold from its equilibrium value leads to a decrease in activation energy for CO_2 hydration, in excellent agreement with the computational results on model ligands (Fig. 3). This strong agreement validates our minimal ligand PES approach. Expansion of the Zn-N bonds to values larger than in the unconstrained, relaxed tetra-aza scaffold instead increase the activation energy. The large energy range (5 kcal/mol) and distance range (0.5 Å) as well as the fact that trends are being compared ensures that this test is a robust one for our approach, despite any residual errors in absolute values of energetics. We find that the dihedrals, which we did not constrain, change from 35° to 12° as the scaffold is squeezed from a Zn-N bond distance of 2.3 to 1.8 Å. The geometry of the scaffold corresponds to flattening of the Zn-N4 dihedral as the lowest energy pathway to shortened Zn-N bonds.

[5] The Zn-N dihedral is not constrained here.

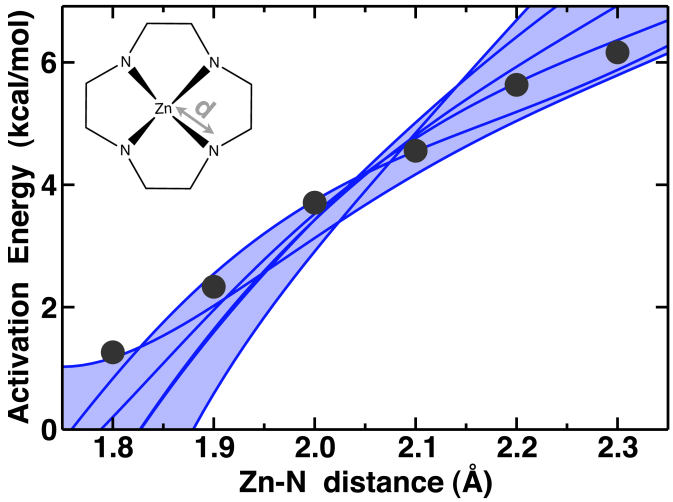

Figure 3. Comparison of activation energy (kcal/mol) for squeezed tetra-aza scaffolds (black circles) with model ligand potential energy surface over a range of 1.8-2.3 Å for the Zn-N bond distances (blue contour lines represent different dihedral values with light blue shading covering the whole range of PES contours).

As an additional test, we considered whether our minimal-ligand PESs could reproduce trends in product release from the squeezed tetra-aza scaffold. Our Zn(II)-$(NH_3)_4$ results suggested a shorter Zn-N bond would facilitate product release (see Table 1). Product release has recently been proposed as the rate limiting step in these small molecule CAII mimics[50]. Comparing product release characteristics for squeezed tetra-aza structures revealed a trend similar to that from the minimal-ligands (Fig. 4). While the absolute agreement is not as impressive as for the activation energies, the trend is consistent across a range of Zn-N distances. Since optimization characteristics observed in the minimal-ligand set were upheld when studying the tetra-aza scaffold under constraint, we

next considered what distance-dependent electronic structure properties were giving rise to this optimization characteristic.

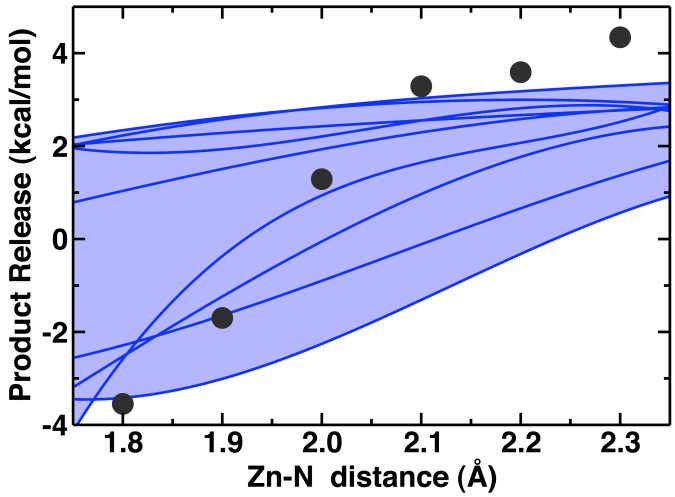

Figure 4. Comparison of product release (kcal/mol) for squeezed tetra-aza scaffolds (black circles) with model ligand potential energy surface over a range of 1.8-2.3 Å for the Zn-N bond distances (blue contour lines represent different dihedral values with light blue shading covering the whole range of PES contours).

In order to identify the electronic structure underpinnings of these trends, we have analyzed the population and molecular orbital character in our minimal-ligand Zn(II)-$(NH_3)_4$ set. When the Zn-N bond is squeezed, the largest changes are a decline in Zn 4*s* population and a commensurate increase in N 2*s* population (Fig. 5). Additionally, 2*s* and 2*p* population for the axial oxygen in the reactant state increases for shorter Zn-N bond distances, while Zn-N 3*d* populations decrease. The overall population trends would suggest that charge is transferred primarily from the Zn metal center to nitrogen, likely through increased bonding interactions between Zn 4*s* and N 2*s*/2*p* as the species are

squeezed together. We also consider the change in the eigenvalues and eigenstates as the model system is squeezed (Fig. 5). Not surprisingly, the energy window for all states with Zn 3*d* character increases as the molecule is squeezed. The most strongly Zn-N distance dependent levels (Fig. 5) have large Zn 3*d* contributions. Bonding orbitals that have strong interactions between N 2*p* and Zn 3*d* are pushed further down in energy upon squeezing, enhancing energetic overlap with deeper N 2*p* and N 2*s* levels. Of the levels that are pushed higher in energy upon squeezing, they all appear to have strong antibonding character between in-plane Zn 3*d*-N 2*p* orbitals. Overall, interactions in the plane between Zn 3*d*/4*s* and N 2*p*/2*s* are strengthened through both charge transfer and better energetic and geometric overlap when the Zn-N bond is squeezed. This strengthening in the plane weakens axial interactions, facilitating turnover through weaker binding of products as well as localizing more charge on the hydroxyl for interaction with CO_2 in the transition state of the hydration reaction.

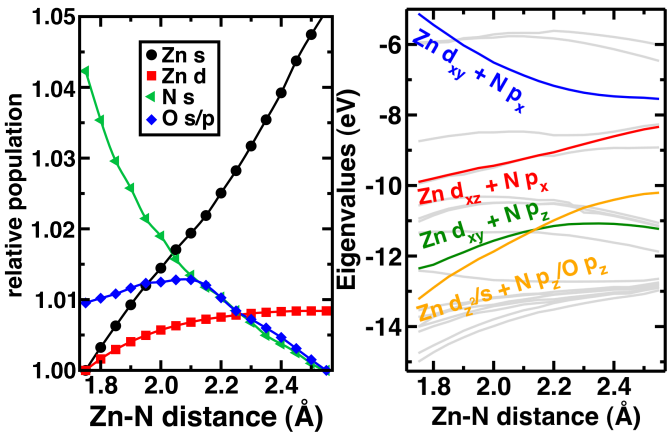

Figure 5. Electronic structure dependence on Zn-N bond distance. (Left) Relative Löwdin charges across a range of Zn-N distances in a four-coordinate, sp^3-N model compound (Zn *s* in black circles has been divided by five to show on the same scale as 3*d* electrons in red

squares). Each curve is set to one at the point where the relative occupation is the smallest across the range of distances. (Right) Variation in eigenvalues across a range of Zn-N distances in a model compound (rapidly varying levels are highlighted in orange, red, green, and blue and labeled with respective atomic contributions).

Following verification of the minimal-ligand PESs, we searched the literature to identify both the spread of Zn-N bonds in experimentally characterized catalysts and the outliers on the tails of this Zn-N distribution. Results of the reaction-oriented potential energy surface analysis have been used as the basis for identifying structures from the Cambridge Structural Database (CSD)[27] that are both potentially suitable candidate catalysts as well as those that oppose the optimization characteristics. A CSD search may be straightforwardly carried out for each metal-ligand combination using the coordination number of the metal and ligand character. In our own searches, we used both native-metal structures (i.e. scaffolds with Zn(II) or Co(II) centers) as well as structures that contained other 3*d* M(II) metals. We identified outliers as structures with metal-ligand distances and dihedrals that are two standard deviations below (Fig. 6a) or above (Fig. 6b) the mean.

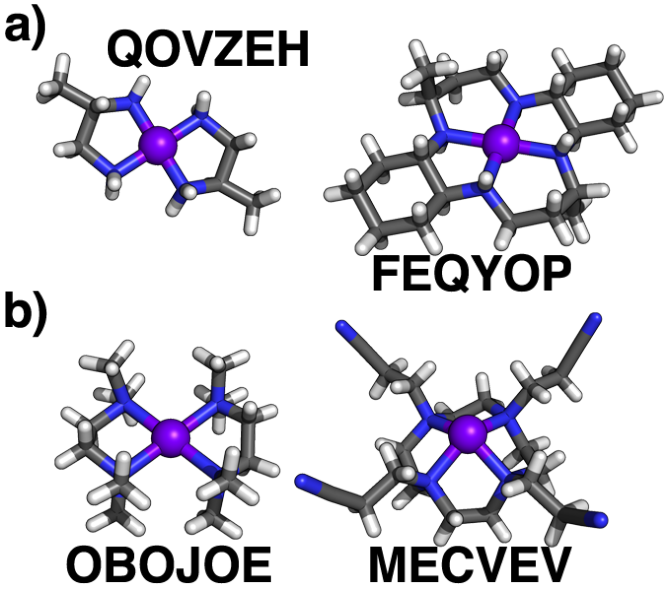

Figure 6. Four-coordinate, sp^3-N structures obtained from database search with Zn-N distances at least (a) two standard deviations below the mean and (b) two standard deviations above the mean Zn-N separation in the distribution of search results and labeled with their CSD structural ID.

Structures that fulfill the optimization vector for Zn(II)-$(NH_3)_4$ were identified in the distribution of structures obtained from the CSD search, while the opposing tail of the distribution was used for control structures. From each of these tails, we selected two structures based on the correspondence between experimentally observed Zn-N bond lengths being within 1% of the calculated bond length (Table 3).

Table 3. Structural and energetic properties of catalysts selected from the database search compared against a reference carbonic anhydrase mimic.

	Ref.	Long Zn-N		Short Zn-N	
	tetra-aza	OBOJOE	MECVEV	QOVZEH	FEQYOP
d(Zn-N) (Å)	2.22	2.27	2.19	1.87	2.07
d(Zn-OH) (Å)	1.86	1.88	1.84	1.90	1.91
$\Delta E_{M\text{-}OH}$ (kcal/mol)	-19.0	-1.5	-32.3	-14.0	-16.4
E_a (kcal/mol)	5.6	16.0	13.0	0.0	3.0
ΔE_{rxn} (kcal/mol)	-11	-8	-2	-15	-17
$D_{e,P}$ (kcal/mol)	4.1	5.3	-22	-9.4	-6.3

As a reference, we use the previously characterized tetra-aza scaffold[51] that we also considered in our constrained Zn-N bond studies. We compare all four reaction characteristics, including the hydroxyl stability and reaction exothermicity steps that we previously identified as not mechanistically relevant. Focusing on the two most relevant reaction characteristics, we observe that the short Zn-N bond structures (CSD IDs: QOVZEH[52] and FEQYOP[53]) are comparable to or improve upon the tetra-aza characteristics, while the long-bonded structures (CSD IDs: OBOJOE[54] and MECVEV[55]) have particularly high activation energies. In one long bond Zn-N structure (CSD ID: MECVEV), the product release is still favorable, while in the other, product release is unfavorable (CSD ID: OBOJOE). This result suggests that steric and electrostatic factors not considered in our PES search or fully modeled by our minimal ligands may come into play in determining these reaction characteristics.

The difference in the results for the two long, Zn-N bond CSD structures becomes apparent in observing differences between structures (Fig. 6b). In one structure, methyl groups on the coordinating nitrogen atoms (CSD ID: OBOJOE) strain the ring, contributing to long Zn-N bonds, while in the other, bulk is added by the scaffold and functionalizing

CN groups (CSD ID: MECVEV). In the MECVEV case, the addition of steric forces from axial CN groups likely destabilizes carbonic acid binding, and eases product release. In fact, we note that we calculate product release in terms of relative binding energy of a water molecule and a carbonic acid molecule, and analysis of the structure of MECVEV suggests steric clashing would be more important with the larger carbonic acid molecule than the relatively smaller water molecule. Thus, it is possible to facilitate product release even while long Zn-N bonds in MECVEV strengthen axial Zn-OH interactions, increasing the activation energy. In the other long Zn-N bond case (CSD ID: OBOJOE), the methyl groups responsible for longer Zn-N bonds are less likely to interfere sterically with an axially bound carbonic acid.

In both short-bonded CSD structures (CSD ID: QOVZEH and FEQYOP), the short bonds are achieved through planar orientation of the ligands with accompanying scaffold features that favor short bonds. For instance, in both QOVZEH and FEQYOP, two five-membered rings are formed with the Zn center, two nitrogen ligands, and two sp^3 carbons from the scaffold. In the case of FEQYOP, the other two rings formed are seven-membered, but this geometry appears to minimize strain on the short Zn-N bonds formed in satisfying the geometric constraints of the other two five-membered rings. Correlated to the observance of short Zn-N bonds, the QOVZEH and FEQYOP structures have longer axial Zn-OH interactions, lower activation energies, and more favorable product release energetics. However, observations of the effect of the bulky axial groups in one long Zn-N bond case (CSD ID: MECVEV) suggests that product release might be further facilitated through some combination of both short Zn-N bonds and axial steric effects, where possible. Future

directions will include a focus on trends in relative binding energies when adding bulky axial groups to scaffold structures either by identifying structures in the literature with bulky axial ligands or through identifying scaffolds that may be straightforwardly functionalized.

4. Conclusions

We have introduced and tested a computational approach for the design and optimization of catalysts. We carried out an optimization scheme for carbon capture catalysts based on the four key characteristics of the CO_2 hydration reaction in carbonic anhydrase and synthetic mimics: 1) reactant hydroxyl formation, 2) CO_2 hydration activation energy, 3) CO_2 hydration reaction step energy, and 4) product release. Using both Zn(II) and Co(II) centers in combination with either four-fold or three-fold sp^3 N or sp^2 N ligands, we observed that steps two and four are key for optimization. We identified the Zn(II)-$(NH_3)_4$ metal/ligand set as both starting from favorable reactivity at its equilibrium geometry as well as having reactivity that can be optimized through variation of structural properties. By constraining a previously characterized tetra-aza scaffold over a range of Zn-N bond lengths, we verified our initial observation that a short bond, shallow dihedral optimization direction improves reaction characteristics. In both the squeezed tetra-aza scaffold and in the model ligand sets, we observed that short Zn-N bonds weakened axial interactions in these catalysts, likely enhancing turnover. This approach of squeezing scaffolds to reduce activation energies, while simply a test of our minimal-ligand

PES approach, could have significant application in embedding catalysts in compressive media[56] or for the use of applied pressure to modify reaction kinetics[57].

Finally, we searched the literature for outlying structures that were both consistent with and opposed to our geometric target. We found that reaction properties, specifically activation and product release energies, for the short Zn-N bond structures were consistent with or improved upon the tetra-aza scaffold reaction energetics. In the long Zn-N bond structures, activation energies were significantly higher, but product release appeared to depend also on the presence of axial scaffold components. Overall, we have presented an alternative approach for identifying catalysts. By seeking out geometric properties that optimize energy-based reaction characteristics, we may now use this information to combinatorially build scaffolds, combine existing literature scaffolds, or design materials that constrain scaffolds away from equilibrium geometries to enhance their reactivity. This approach, now validated for CO_2 hydration, should have significant promise for catalyst design in other reactions.

5. Acknowledgments

This work was partly performed under the auspices of the U.S. Department of Energy by the Lawrence Livermore National Laboratory under Contract No. DE-AC52-07NA27344. This project was funded by Laboratory Directed Research and Development 10-ERD-035. HJK holds a Career Award at the Scientific Interface from the Burroughs Wellcome Fund. The use of computer resources from the Lawrence Livermore National Laboratory is gratefully acknowledged.

Supporting Information Available.

References

[1] M.J. Baldwin, V.L. Pecoraro, Journal of the American Chemical Society, 118 (1996) 11325.

[2] V. Balzani, S. Campagna, G. Denti, A. Juris, S. Serroni, M. Venturi, Accounts of Chemical Research, 31 (1998) 26.

[3] H.U. Blaser, F. Spindler, M. Studer, Applied Catalysis A: General, 221 (2001) 119.

[4] R. Pachauri, A. Reisinger, Intergovernmental Panel on Climate Change, (2007).

[5] J.D. Figueroa, T. Fout, S. Plasynski, H. McIlvried, R.D. Srivastava, International Journal of Greenhouse Gas Control, 2 (2008) 9.

[6] L. Bao, M.C. Trachtenberg, Journal of Membrane Science, 280 (2006) 330.

[7] R.G. Khalifah, Journal of Biological Chemistry, 246 (1971) 2561.

[8] H. Steiner, B.H. Jonsson, S. Lindskog, European Journal of Biochemistry, 59 (1975) 253.

[9] S. Lindskog, Pharmacology & Therapeutics, 74 (1997) 1.

[10] K. Hakansson, M. Carlsson, L.A. Svensson, A. Liljas, Journal of Molecular Biology, 227 (1992) 1192.

[11] A. Liljas, S. Lovgren, P.C. Bergsten, U. Carlbom, M. Petef, I. Waara, Strandbe.B, K. Fridborg, L. Jarup, K.K. Kannan, Nature-New Biology, 235 (1972) 131.

[12] V.M. Krishnamurthy, G.K. Kaufman, A.R. Urbach, I. Gitlin, K.L. Gudiksen, D.B. Weibel, G.M. Whitesides, Chemical Reviews, 108 (2008) 946.

[13] G. Parkin, Chemical Reviews, 104 (2004) 699.

[14] X.P. Zhang, R. Vaneldik, Inorganic Chemistry, 34 (1995) 5606.

[15] X.P. Zhang, R. Vaneldik, T. Koike, E. Kimura, Inorganic Chemistry, 32 (1993) 5749.

[16] D.N. Silverman, S. Lindskog, Accounts of Chemical Research, 21 (1988) 30.

[17] S. Lindskog, P.O. Nyman, Biochimica Et Biophysica Acta, 85 (1964) 462.

[18] K.A. Kogut, R.S. Rowlett, Journal of Biological Chemistry, 262 (1987) 16417.

[19] S.R. Powell, The Journal of Nutrition, 130 (2000) 1447S.

[20] L. Guidoni, K. Spiegel, M. Zumstein, U. Röthlisberger, Angewandte Chemie International Edition, 43 (2004) 3286.

[21] J.K. Norskov, T. Bligaard, J. Rossmeisl, C.H. Christensen, Nature Chemistry, 1 (2009) 37.

[22] L.E. Orgel, An introduction to transition-metal chemistry: ligand-field theory Wiley, New York, 1961.

[23] P. Giannozzi, S. Baroni, N. Bonini, M. Calandra, R. Car, C. Cavazzoni, D. Ceresoli, G.L. Chiarotti, M. Cococcioni, I. Dabo, A. Dal Corso, S. de Gironcoli, S. Fabris, G. Fratesi, R. Gebauer, U. Gerstmann, C. Gougoussis, A. Kokalj, M. Lazzeri, L. Martin-Samos, N. Marzari, F. Mauri, R. Mazzarello, S. Paolini, A. Pasquarello, L. Paulatto, C. Sbraccia, S. Scandolo, G. Sclauzero, A.P. Seitsonen, A. Smogunov, P. Umari, R.M. Wentzcovitch, Journal of Physics-Condensed Matter, 21 (2009) 395502.

[24] J.P. Perdew, K. Burke, M. Ernzerhof, Physical Review Letters, 77 (1996) 3865.

[25] H.J. Kulik, N. Marzari, J. Chem. Phys., 133 (2010) 114103.

[26] G. Makov, M.C. Payne, Physical Review B, 51 (1995) 4014.

[27] D.A. Fletcher, R.F. McMeeking, D. Parkin, Journal of Chemical Information and Computer Sciences, 36 (1996) 746.

[28] I.J. Bruno, J.C. Cole, P.R. Edgington, M. Kessler, C.F. Macrae, P. McCabe, J. Pearson, R. Taylor, Acta Crystallographica Section B-Structural Science, 58 (2002) 389.

[29] N.N. Greenwood, Chemistry of the Elements, 1997.

[30] K. Adamczyk, M. Pr√©mont-Schwarz, D. Pines, E. Pines, E.T.J. Nibbering, Science, 326 (2009) 1690.

[31] T. Bally, G.N. Sastry, The Journal of Physical Chemistry A, 101 (1997) 7923.

[32] B. Braida, P.C. Hiberty, A. Savin, The Journal of Physical Chemistry A, 102 (1998) 7872.

[33] Y.K. Zhang, W.T. Yang, J. Chem. Phys., 109 (1998) 2604.

[34] K. Exner, P.v.R. Schleyer, The Journal of Physical Chemistry A, 105 (2001) 3407.

[35] J. Grafenstein, E. Kraka, D. Cremer, J. Chem. Phys., 120 (2004) 524.

[36] S. Petrie, R. Stranger, Inorganic Chemistry, 43 (2004) 2597.

[37] D.J. Tozer, F. De Proft, The Journal of Physical Chemistry A, 109 (2005) 8923.

[38] A.D. Dutoi, M. Head-Gordon, Chemical Physics Letters, 422 (2006) 230.

[39] P. Mori-Sanchez, A.J. Cohen, W.T. Yang, J. Chem. Phys., 125 (2006).

[40] A.J. Cohen, P. Mori-Sanchez, W. Yang, Science, 321 (2008) 792.

[41] A. Lange, J.M. Herbert, Journal of Chemical Theory and Computation, 3 (2007) 1680.

[42] A. Togni, L.M. Venanzi, Angewandte Chemie International Edition in English, 33 (1994) 497.

[43] J.E. Coleman, Journal of Biological Chemistry, 242 (1967) 5212.

[44] J.E. Coleman, Nature, 214 (1967) 193.

[45] B.L. Vallee, A. Galdes, Advances in Enzymology and Related Areas of Molecular Biology, 56 (1984) 283.

[46] W.N. Lipscomb, Annual Review of Biochemistry, 52 (1983) 17.

[47] S.J. Lippard, J.M. Berg, Principles of Bioinorganic Chemistry, 1994.

[48] W. Maret, Journal of Trace Elements in Medicine and Biology, 19 (2005) 7.

[49] S.E. Wong, E.Y. Lau, H.J. Kulik, J.H. Satcher, C. Valdez, M. Worsely, F.C. Lightstone, R. Aines, Energy Procedia, 4 (2011) 817.

[50] L. Koziol, C.A. Valdez, S.E. Baker, E.Y. Lau, W.C. Floyd, S.E. Wong, J.H. Satcher, F.C. Lightstone, R.D. Aines, Inorganic Chemistry, 51 (2012) 6803.

[51] J.H. Satcher Jr, S.E. Baker, H.J. Kulik, C.A. Valdez, R.L. Krueger, F.C. Lightstone, R.D. Aines, Energy Procedia, 4 (2011) 2090.

[52] B.-Z. Lin, L.-W. He, B.-H. Xu, X.-L. Li, Z. Li, P.-D. Liu, Crystal Growth & Design, 9 (2008) 273.

[53] K.Y. Choi, I.H. Suh, J.R. Park, Main Group Metal Chemistry, 21 (1998) 783.

[54] D.A. Handley, P.B. Hitchcock, G.J. Leigh, Inorganica Chimica Acta, 314 (2001) 1.

[55] D.-Y. Kong, L.-H. Meng, J. Ding, Y.-Y. Xie, X.-Y. Huang, Polyhedron, 19 (2000) 217.

[56] C.R. Bamford, Phys. Chem. Glasses, 3 (1962) 189.

[57] A. Streitwieser Jr., Taft, R. W., and le Noble, W. J., Kinetics of Reactions in Solutions Under Pressure, in: Progress in Physical Organic Chemistry John Wiley & Sons, Inc., 1967, pp. 207.